Earth and Planetary Science Letters 385 (2014) 59–67

Contents lists available at ScienceDirect

Earth and Planetary Science Letters

www.elsevier.com/locate/epsl

Prolonged eruptive history of a compound volcano on Mercury: Volcanic and tectonic implications

David A. Rothery [a,*], Rebecca J. Thomas [a], Laura Kerber [b]

[a] Department of Physical Sciences, The Open University, Milton Keynes, MK7 6AA, UK
[b] Laboratoire de Météorologie Dynamique du CNRS, Université Paris 6, Paris, France

ARTICLE INFO

Article history:
Received 6 April 2013
Received in revised form 26 September 2013
Accepted 9 October 2013
Available online 8 November 2013
Editor: C. Sotin

Keywords:
Mercury
volcanism
compound volcano
Caloris basin
MESSENGER

ABSTRACT

A 27 × 13 km 'rimless depression' 100 km inside the southwest rim of the Caloris basin is revealed by high resolution orbital imaging under a variety of illuminations to consist of at least nine overlapping volcanic vents, each individually up to 8 km in diameter. It is thus a 'compound' volcano, indicative of localised migration of the site of the active vent. The vent floors are at a least 1 km below their brinks, but lack the flat shape characteristically produced by piston-like subsidence of a caldera floor or by flooding of a crater bottom by a lava lake. They bear a closer resemblance to volcanic craters sculpted by explosive eruptions and/or modified by collapse into void spaces created by magma withdrawal back down into a conduit. This complex of overlapping vents is at the summit of a subtle edifice at least 100 km across, with flank slopes of about only 0.2 degrees, after correction for the regional slope. This is consistent with previous interpretation as a locus of pyroclastic eruptions. Construction of the edifice could have been contributed to by effusion of very low viscosity lava, but high resolution images show that the vent-facing rim of a nearby impact crater is not heavily embayed as previously supposed on the basis of lower resolution flyby imaging. Contrasts in morphology (sharpness versus blurredness of the texture) and different densities of superposed sub-km impact craters inside each vent are consistent with (but do not prove) substantial differences in the age of the most recent activity at each vent. This suggests a long duration of episodic magmagenesis at a restricted locus. The age range cannot be quantified, but could be of the order of a billion years. If each vent was fed from the same point source, geometric considerations suggest a source depth of at least 50 km. However, the migration of the active vent may be partly controlled by a deep-seated fault that is radial to the Caloris basin. Other rimless depressions in this part of the Caloris basin fall on or close to radial lines, suggesting that elements of the Pantheon Fossae radial fracture system that dominates the surface of the central portion of the Caloris basin may continue at depth almost as far as the basin rim.

© 2013 Elsevier B.V. All rights reserved.

1. Introduction

The vent complex on which we focus here is located at 22.3°N, 146.2°E, situated about 100 km inside the southwestern rim of Mercury's Caloris basin. It was discovered in images returned during MESSENGER's first flyby in 2008 (Fig. 1), and described by Head et al. (2008) as a 'kidney-shaped depression' surrounded by a relatively bright deposit with diffuse outer edges that they interpreted to be pyroclastic deposits erupted from the vent area. They referred to it as a 'rimless depression', on the grounds of lacking any trace of a rampart or elevated rim such as surrounds an impact crater. In the then absence of altimetric data, Head et al. (2008) used indirect evidence to infer that the overall structure is a 'broad, low shield volcano'. The inferred pyroclastic deposit centred on the vent was listed as Red Spot 3 (RS-03) by Blewett et al. (2009) in their preliminary analysis of colour trends, and investigated as an example of evidence for unexpectedly high volatile content in the erupting magma (3600–13,000 ppm) by Kerber et al. (2009). With a radius of 24 km, this is the 5th most areally extensive candidate pyroclastic deposit documented during the three MESSENGER flybys (Kerber et al., 2011).

As well as presenting several other examples of volcanic vents, Head et al. (2009) suggested that the scalloped edges of the RS-03 rimless depression are a result of 'successive stages of inflation and collapse of the (magma) reservoir' leading to 'multiple intersecting depressions'. Here we take advantage of higher resolution images and altimetric data acquired during MESSENGER's first three Mercury solar days in orbit to provide a more complete account of this feature. Diverse ages of the individual vents demonstrate a prolonged, or at least complicated, history of episodic eruption involving migration of the locus of eruption to and fro by about 25 km. A hitherto unrecognised vent extends the rimless

* Corresponding author. Tel.: +44 1908 652124; fax: +44 1908 655151.
E-mail address: d.a.rothery@open.ac.uk (D.A. Rothery).

0012-821X/$ – see front matter © 2013 Elsevier B.V. All rights reserved.
http://dx.doi.org/10.1016/j.epsl.2013.10.023

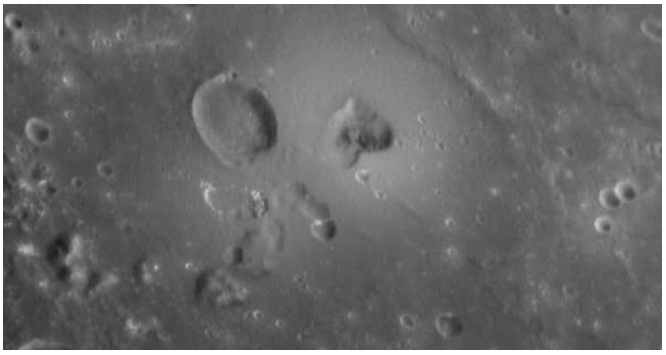


Fig. 1. MESSENGER flyby 1 'discovery' image, as used in Head et al. (2008). The "kidney-shaped" volcanic depression is in the upper centre, a 25 km circular impact crater lies to its west, and several smaller putative volcanic craters lie to the southwest.

depression further west than previously realised, so it can no longer be aptly described as 'kidney-shaped'. We discuss first this main vent complex, and then draw attention to its relationship to other rimless depressions nearby. Because this feature has previously been classified as a 'rimless', we use the term 'brink' rather than 'rim' to refer to the perimeter of the depression.

2. Insights from orbit

2.1. High-resolution imaging

The imaging system on MESSENGER is MDIS, the Mercury Dual Imaging System (Hawkins et al., 2007). It consists of a monochrome narrow angle camera (NAC) and a multispectral wide angle camera (WAC). The RS-03 vent complex was imaged three times by targeted high-resolution NAC acquisitions during MESSENGER's first three solar days orbit, and there are many WAC images that also show more detail than the flyby images. We show in Fig. 2a a WAC mosaic of the region and in Fig. 2b a map of the same area marking the RS-03 vent complex and five other rimless depressions. An inset on the map assigns a letter to each vent within RS-03 for ease of reference.

Spatial resolution in the NAC images is tremendously improved compared to the flyby imaging, and the variety of solar illumination conditions allows many further insights. All three NAC acquisitions were by off-nadir viewing (emission angles between 30 and 46 degrees). Attributes of these images and one particularly useful WAC image are listed in Table 1, and geo-rectified mosaics centred on each are shown in Fig. 3.

The view in Fig. 3a was acquired under conditions of solar illumination similar to those in the flyby image (Fig. 1), with the Sun high in the east. However, its significantly higher resolution reveals very clearly some textural contrasts within the vent complex that could not previously be recognised. The sides and floors of pits occupying the east, north and west of the complex are smooth. These are A–E on Fig. 2b, although A is scarcely distinguishable (the brink of the depression seeming to be at the western edge of B and C) and might not have been recognised if this had been

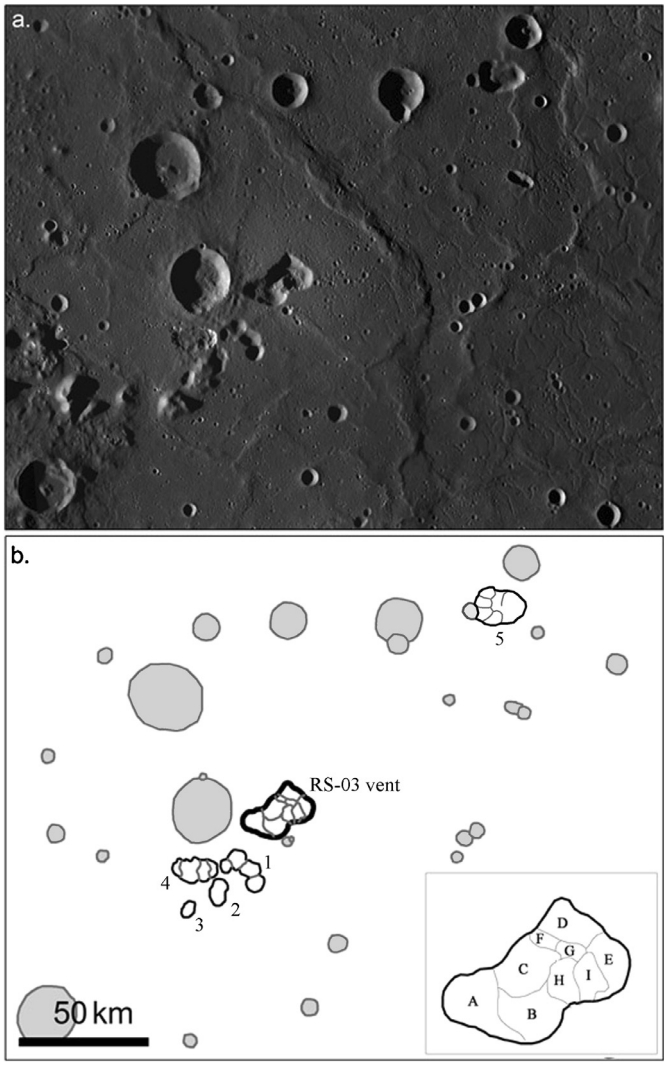


Fig. 2. (a) Regional mosaic of WAC images mapped to a sinusoidal projection centred on the RS-03 vent complex. (b) Sketch map of the area shown in (a), based on NAC and WAC images. The main vent complex (RS-03) is shown with a heavy black outline. Other rimless depressions hosting possible vents are outlined with a finer black boundary, and numbered 1–5. Septa marking the divides between individual vents marked by fine grey lines. Impact craters are shown with a grey fill. The inset shows the main vent complex enlarged, and with letters to identify each vent. The original description as 'kidney shaped' (Head et al., 2008) was based on the outline around vents B–I only, because vent A was not apparent in the flyby image (Fig. 1). Boundaries between vents within vent complex 5 were drawn on the basis of targeted NAC images that became available while this paper was in review; see Supplementary Material.

the only illumination available. We interpret each of A–E as hosting at least one volcanic vent. In the centre of the complex is an area of much finer texture, whose outline and internal morphology suggest that it contains at least four overlapping vents (F–I on Fig. 2b). Cross-cutting relationships demonstrate that these are younger than their smoother-textured neighbours. The rough tex-

Table 1
MESSENGER MDIS NAC and WAC orbital images used in this study.

Image ID	Solar incidence angle (degrees)	Solar azimuth (degrees)	Emission angle (degrees)	Spacecraft azimuth (degrees)	Raw pixel size (m)
EN0215894570M	39.6	133.6	45.5	333.9	28.6
EN0220591242M	74.5	264.8	41.0	359.9	20.7
EN0220850481M	83.7	267.8	30.1	179.0	19.5
EW0220764090G	79.7	266.0	1.6	351.9	125.1

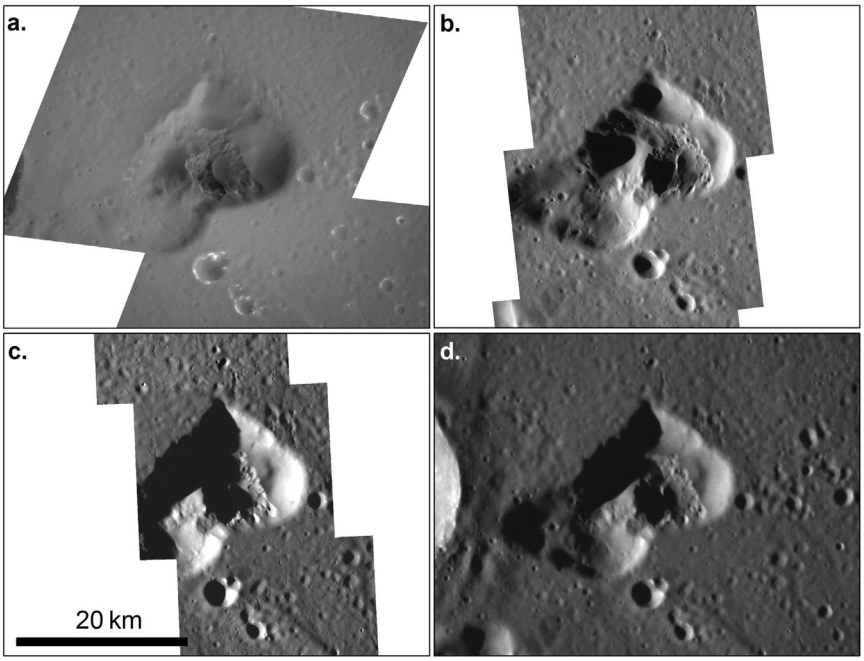


Fig. 3. Mosaics of NAC (a–c) and WAC (d) images of the RS-03 vent area, including the individual frames listed in Table 1. These are mapped to the same sinusoidal projection as Fig. 2. The frame including all or most of the vent in each case is: (a) EN0215894570M, (b) EN0220591242M, (c) EN0220850481M, (d) EW0220764090G.

ture within vents F–I suggests that they were active more recently than the smoother-textured vents. We discuss the possible nature of this activity in Section 4, where we argue that the smoother-textured vents A–E were formerly much rougher, and that their contours have become muted. Such smoothing is likely to occur over time by some combination of mantling by younger pyroclastic deposits and regolith-forming impacts.

The view in Fig. 3b was acquired when the Sun was considerably lower and in the west. This illumination accentuates the textural contrast between older and younger vents, and there are shadows from which depths can be estimated. Moreover, the favourable shading under this illumination direction reveals a westward extension of the overall rimless depression that destroys its kidney-like shape. We interpret this as another vent belonging to the complex (A on Fig. 2b), and note that it contains several sub-km sized impact craters on its floor, which are less common or absent in the other vents. These craters exhibit a range of degradation states, from sharp to muted, and so are almost certainly of different ages.

The floor area of vent A is too small for reliable statistics, but it is notable that the crater-density there is not significantly different from that on nearby surfaces outside the rimless depression, and there is no obvious increase in superposed crater density with distance away from the brink. The fresher craters in particular are clustered and are therefore likely to be secondaries, and so of little use for relative dating, especially of areas so small as the interior of a vent (e.g., McEwen and Bierhaus, 2006). However cross-cutting relationships also suggest that vent A is the oldest in the complex, and it is plausible that vent A ceased activity not very long after the formation of the adjacent plains, and did so significantly longer ago than other vents in the complex. Comparative preservation state suggests that its immediate neighbour to the southeast, vent B, may be the next-oldest.

The view in Fig. 3c was acquired under the highest incidence angle (most grazing-incidence sunlight) of the set. It misses the western vent, but the longer shadows and different viewing geometry (spacecraft azimuth in Table 1) accentuate some features of the central vents F–I that are less apparent in the other views.

Slopes that appeared foreshortened or elongated in the raw NAC images because of the off-nadir viewing geometry remain distorted in the geo-rectified images. Therefore we show as Fig. 3d a geo-rectified WAC image in which the entire interior of the vent complex is covered by a single WAC frame acquired with near-nadir viewing geometry (emission angle 1.6 degrees) but with similar conditions of solar illumination to two of the NAC images (Table 1). This shows the plan-view shapes of the steep, young vents F–I with minimal distortion. It provides confirmation of the western vent (A), and shadowing on the southeastern part of its floor hints at structural complexity that may indicate at least one additional vent contained within it.

The largest vents A, B and C are each about 9 km across, but may have been slightly bigger before being cut across by younger vents. The average spacing between centres of adjacent vents is 5.5 km (with a range from 3.9 km to 9.9 km). This may equate to the average spacing between conduits, though it is conservatively large given that vent A could in fact comprise more than one individual vent.

2.2. Topography

Because of its between-track spacing at these latitudes, Mercury Laser Altimeter (MLA) gridded topography (Zuber et al., 2012) has a spatial resolution that is too coarse to test the inference made by Head et al. (2008) that the RS-03 vent complex is at the summit of a feature that is 'domelike in nature'. Moreover, the volcanically-flooded floor of the Caloris basin has been warped by the imposition of long wavelength topography (Oberst et al., 2010; Zuber et al., 2012) on a scale of several hundreds of km, as well as being distorted more locally by wrinkle ridges.

Fortunately, the 400 m along-track spacing of MLA data points is adequate to reveal smaller-scale topography in the along-track direction. Three MLA tracks cross the centre of our region of interest (Fig. 4). One of these crosses the RS-03 vent complex, and the other two graze its northeastern brink. Data from the vent-crossing track provide a good measurement of the depth of the northernmost vent (D), bottoming out before ground returns are lost, showing its floor to be 1.0 km below the northern brink. There

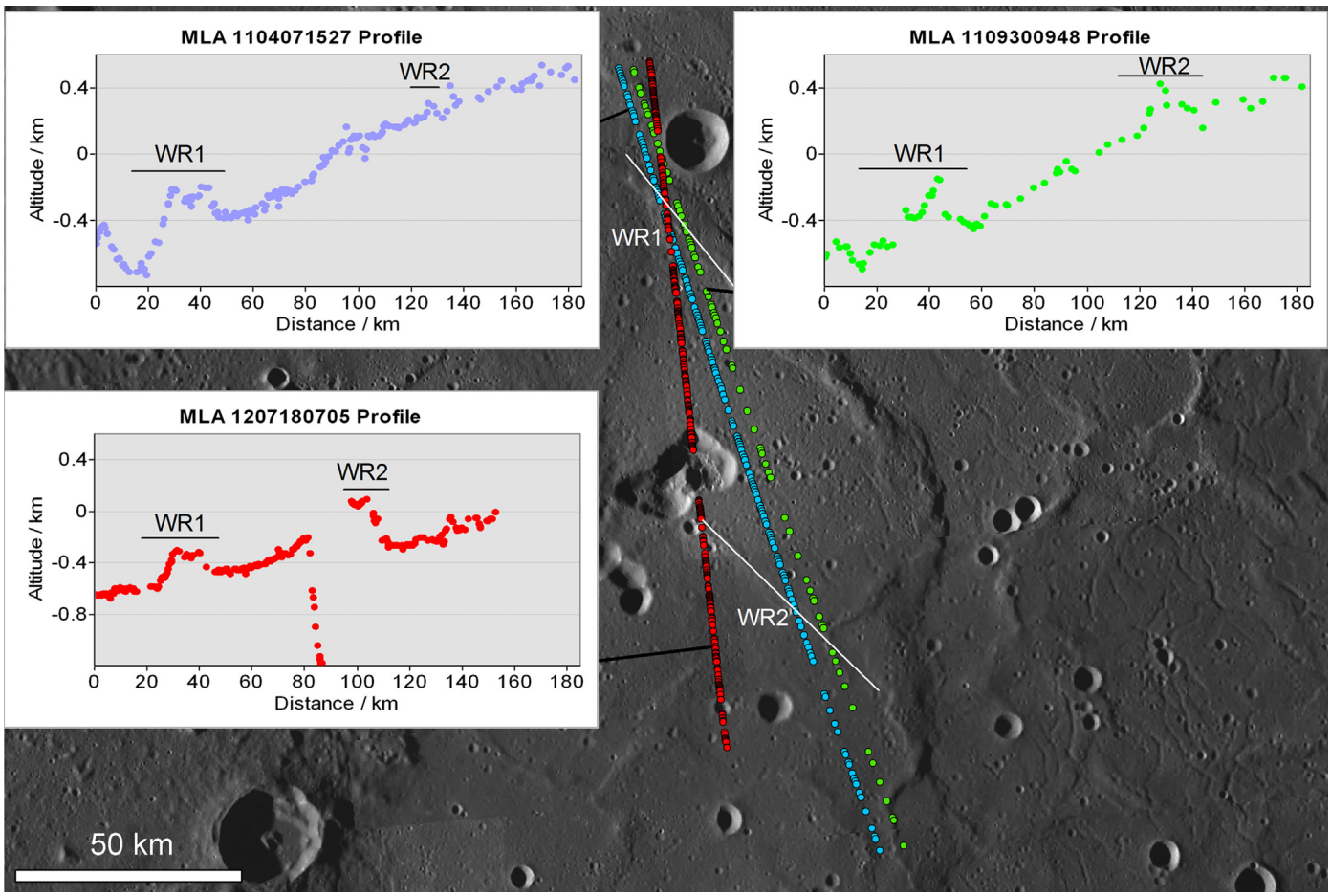


Fig. 4. MLA profiles crossing or passing near to the RS-03 vent complex. All usable (non-noise trigger channels) shot points are shown. WR1 is a major wrinkle ridge and WR2 is a less prominent wrinkle ridge. The portions of each altimetry profile affected by the wrinkle ridges are marked accordingly. Note the gap in data in the vent-crossing line.

are no usable MLA returns inside the rest of the vent complex (the track crosses vents G and H), but reliable data show the southern brink to be more than 0.2 km higher than the northern brink. This may in part be because a minor wrinkle ridge (WR2 on Fig. 4) intersects the brink of the complex near here.

Although the slope down into the vent from the brink looks steep on the profile in Fig. 4, the scale is vertically exaggerated. In fact, the average slope from the brink to the deepest point is only about 9°. Vent D measures 7.7 km by 5.1 km, and using the mean value as its diameter, we find a depth/diameter ratio of 0.16.

It is clear from visual appearance on the images (Fig. 3) and on the MLA profile of vent D (Fig. 4) that the vents within this complex are not flat-floored, but have bowl-shaped or V-shaped profiles. The within-vent shadows cast at high solar incidence angle (Fig. 3b and c) allow depths of several of the vents to be measured. These are minimum depths, because in most cases the shadow terminus is likely to be part-way up the opposite, Sun-facing, wall rather than coinciding with the vent bottom. We obtain minimum depths in the range 0.6–1.7 km for all shadowed vents in Fig. 3b and c. Some depths are below an internal septum (between C and H, and between H and I) rather than below the external brink of the complex, so that the depth below the brink is likely to be somewhat greater.

At first sight, no MLA profile shows obvious evidence of the vent complex being at the summit of a volcanic edifice. Topography outside the vents is dominated by wrinkle ridges and impact craters. However, there is an along-profile regional slope of about 0.4° downwards towards the north. De-trending of the profiles to remove the regional slope (Fig. 5) reveals an along-track slope of about 0.21° downwards to the north from the northern brink of the vent complex and about 0.07° downwards to the south from its southern brink. If the regional tilt post-dates volcanic activity as deduced on various grounds by Zuber et al. (2012), this represents the original flank slopes on either side of the vent complex. Original slopes could be symmetrical at 0.14° on either flank if we have slightly overestimated the regional slope, which could easily be the case given the complications arising from the wrinkle ridge adjacent to the north. However, slopes are clearly very gentle, irrespective of whether or not they are symmetrical on either side. Such a flank gradient is considerably less steep than for the majority of low basaltic shields on Mars, where for example Hauber et al. (2009) report a range of 0.3–4.7° on the upper flanks of 24 examples in the Tempe province.

2.3. Nearby related vents

Travelling southwest from the brink of the RS-03 complex, the first feature of note is a curved line of four or five overlapping craters, each roughly circular and 5–10 km in diameter. Head et al. (2008, 2009) mapped this group as an irregularly shaped depression and regarded it as of likely volcanic origin. This is prominent in Fig. 6 and is the feature labelled 1 on Fig. 2b. These craters lack obvious rims and we agree that they are possibly, though not necessarily, of volcanic rather than impact origin, as are two similar depressions to their southwest (2 and 3 on Fig. 2b) that were also mapped by Head et al. (2008, 2009) and which lack circular substructures.

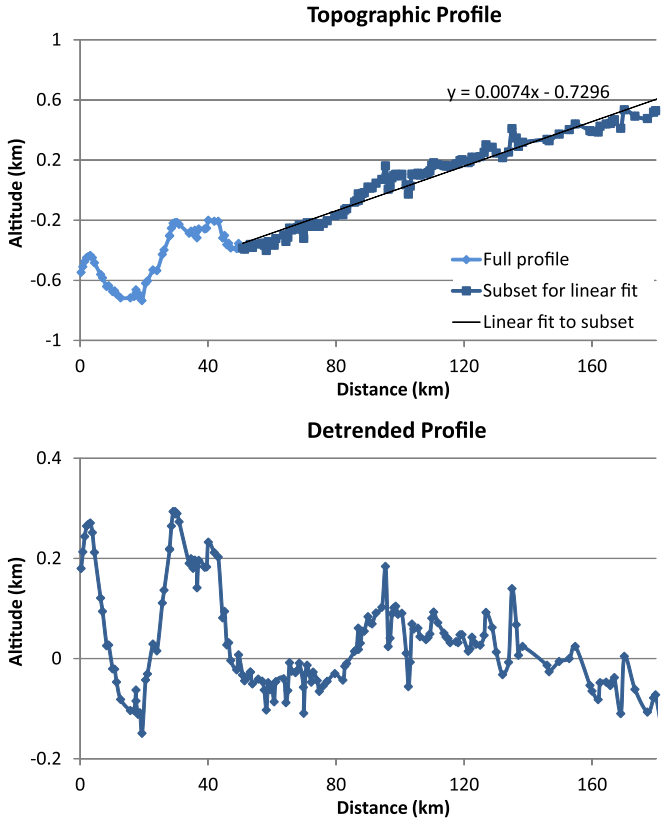


Fig. 5. (Top) MLA profile 1104071527 (see Fig. 3) indicating the region unaffected by wrinkle ridges used to define the regional slope. (Bottom) De-trended to reveal the flank slopes of the edifice, on the assumption that the regional tilt was imposed after edifice growth. The wrinkle ridge at the north (left) end is a more significant topographic feature than the RS-03 volcanic edifice, which occurs at 80–160 km along the track. This profile is tangential to the brink of the rimless depression, and so does not show the vents.

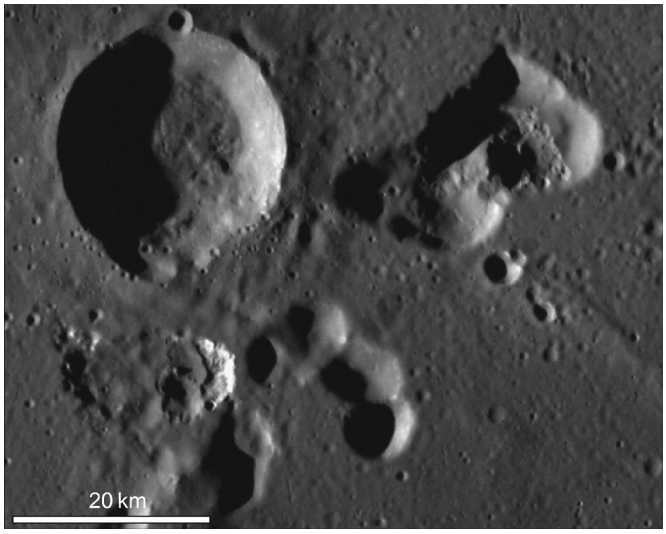


Fig. 6. WAC mosaic (sinusoidal projection) showing the RS-03 vent complex in context with its southwestern neighbours.

Of less equivocal volcanic origin is the shallow 20 × 10 km, roughly rectangular, rimless depression with finely-scalloped walls that is immediately adjacent (4 on Fig. 2b). This is the centre of a candidate pyroclastic deposit, with a 'pyroclastic' spectral signature, listed as RS-03 SW by Kerber et al. (2011). The easternmost pit on its floor can be seen to contain high-albedo material similar to that found associated with areas of hollow-formation (Blewett et al., 2011, 2013), which we have found (Thomas et al., 2013) to be widely associated with rimless depressions elsewhere on Mercury. There seem to be at least four vents within 'feature 4', of which the deepest, and perhaps youngest, are at either end.

We draw special attention to a newly-identified 19 × 13 km rimless depression that lies 120 km to the northeast of the RS-03 vent, which is labelled 5 on Fig. 2b. A fortuitously well-placed and low-noise MLA track crosses this feature, as illustrated in Fig. 7. It passes very close to what appears to be the deepest part of the easternmost vent within the 'feature 5' complex, and the profile (Fig. 7b) shows it to have sloping sides and a narrow bottom. The steepness is exaggerated in Fig. 7b, and in fact the slope from the northern brink to the deepest point is an average of 7° (and steeper near the top), whereas the opposite slope as 17°. The deepest point on the profile is about 1.3 km below the brink. Given that the profile may not cross the deepest point in the vent, a minimum depth/diameter ratio is 0.13.

After de-trending to remove the regional slope (Fig. 7c), the outward slope downward to the north from the northern brink can be seen to be about 0.30 km in 50 km, while the outward downward slope to the south from the southern brink is about 0.22 km in 50 km. The flank slopes are thus about 0.34° on the north and 0.25° on the south. This is marginally steeper than the flank slopes of the RS-03 complex, but less steep than the majority of low basaltic shields on Mars (Hauber et al., 2009).

'Feature 5' has no surrounding spectral anomaly in WAC colour, and lacks any other evidence of pyroclastic activity, but is otherwise similar to feature 4, including being apparently deepest at either end.

Targeted NAC images of 'feature 5' acquired in June and July 2013 became available on the MESSENGER website while this paper was under review (see Supplementary Material), and provided the basis for the internal boundaries between the vents within it shown in Fig. 2. Stereoscopic viewing confirms that the MLA track in Fig. 7 passes close to the deepest point of the easternmost vent. There is no topographically rough area analogous to vents F–I within the RS-03 complex within feature 5, and the whole floor is liberally peppered by sub-1 km impact craters.

3. Tectonic implications

There is a radial fracture system named Pantheon Fossae at the middle of the Caloris basin (Murchie et al., 2008), and the extension of a line drawn through the long axis of the RS-03 vent complex leads towards the centre of the pattern, as illustrated in Fig. 8. 'Feature 4' (which, as already noted, has a surrounding pyroclastic deposit) lies exactly on this line, and 'feature 5' lies close to it.

Head et al. (2009) note additional rimless depressions, many with associated candidate pyroclastic deposits, close inside the Caloris rim between 200 and 700 km southeast of RS-03. The closest group of these includes a vent surrounded by candidate pyroclastic deposit RS-03 SE of Kerber et al. (2011). These fall within the area of Fig. 8 and are identified on the inset map. Four rimless depressions in this group, including the one centred within candidate pyroclastic deposit RS-03 SE, fall along a second line radial to Caloris.

The Pantheon Fossae radial fractures can be traced outwards to about 55% of the basin radius, where they are replaced by circumferential fractures, whereas the tectonic pattern beyond 70% of the radius is dominated by randomly-oriented ridges attributable to contraction (Byrne et al., 2013a, 2013b). Our two lines extending the vent alignment inwards are parallel to the first clear surficial radial fractures that they encounter (i.e., those most distal from the basin centre), which lends weight to their inferred association. Within about 150 km of the basin centre the 'radial' fractures in

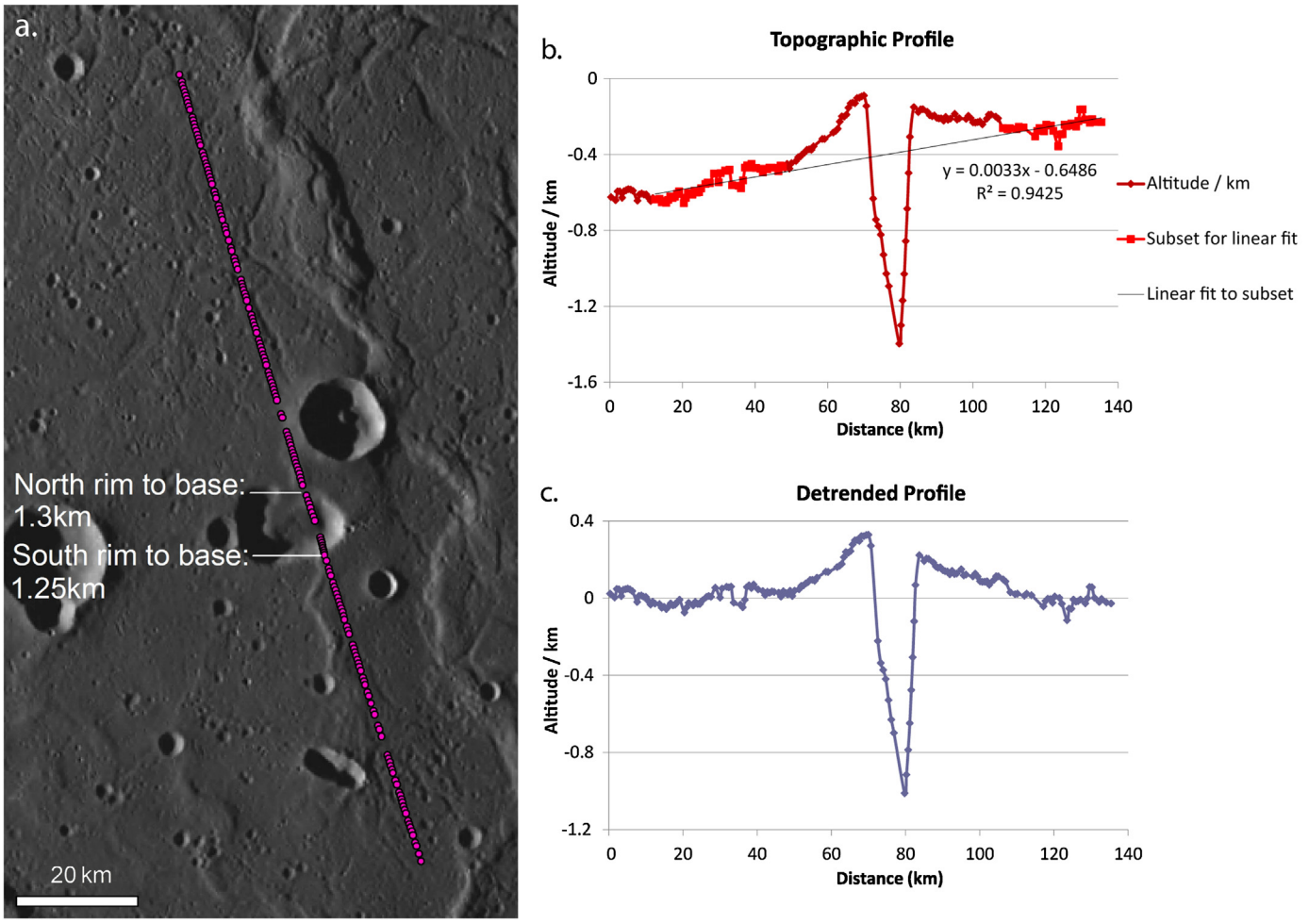


Fig. 7. (a) MDIS9 mosaic showing the location of MLA track 1104070323 that crosses rimless depression 5 (Fig. 2b). (b) The MLA profile indicating the region unaffected by wrinkle ridges used to define the regional slope. (c) The wrinkle-ridge free portion of (b) de-trended to reveal the flank slopes of the edifice.

this part of the pattern bend gradually to the right by about 10°, and because of this our two lines meet a few tens of km north of where the fracture pattern converges.

The consensus interpretation of Pantheon Fossae is that they are grabens, representing radial extension. Basilevsky et al. (2011) claim that these radial grabens are the oldest tectonic element in Caloris, whereas Watters et al. (2009) and Byrne et al. (2013a) consider that extensional features in Caloris post-date the contractional ridges. Head et al. (2008) suggested that the Pantheon Fossae grabens overlie dykes, although other interpretations are possible, such as fracturing in response to the impact that formed Apollodorus crater (Freed et al., 2009), which is suspiciously close to the centre of the pattern.

The fact that the RS-03 vent complex is radially elongated suggests that its magma supply rose up a radial fracture. The occurrence of the associated vents very close to the same line suggest that this fracture could be at least 160 km long, and may even extend all the way from the centre of the basin, which would make it more than 800 km long. A similar argument can be made for the alignment of rimless depressions that includes candidate pyroclastic deposit RS-03 SE (Fig. 8). If this interpretation is correct, it could mean that, in the outer 45% of Caloris, radial extensional tectonism occurred at depth but never propagated to the surface with sufficient strain to form grabens. Alternatively, radial extensional tectonism could pre-date a more recent regional volcanic resurfacing event in the outer part of Caloris, which buried any surface expressions of radial tectonics that had occurred before cessation of vent activity. In the latter case, given that compressional tectonism is apparent on surfaces in the outer region of Caloris, it would lend weight to the argument by Basilevsky et al. (2011) that radial extension pre-dates other tectonic events.

The Caloris Basin has several other candidate vents round much of its circumference, but all are close to the edge of the basin. Our 'feature 5', about 220 km from the basin rim, is the furthest inwards from the rim that we have identified. Thicker basin-filling lavas towards the centre of the basin (Byrne et al., 2013b) may have acted as a cap to prevent vent-forming eruptions. Alternatively there may be additional structural control on magma ascent by circumferential fractures close to the basin rim, similar to that suggested to explain the locations of large shield volcanoes peripheral to some deeply-flooded lunar impact basins (Spudis et al., 2013). A case could be made that the alignment of the four most distal candidate vents in the Fig. 8 inset is controlled by such a circumferential fracture.

4. Eruptive history

4.1. The RS-03 vent complex

The locus of volcanic activity in the RS-03 vent complex has evidently migrated over time, with the most recent activity being near the centre. The most appropriate term to describe an edifice hosting such a vent complex is 'compound volcano', defined by Davidson and de Silva (2000) as a 'volcanic massif formed from coalesced products of multiple, closely spaced, vents.' This is not to

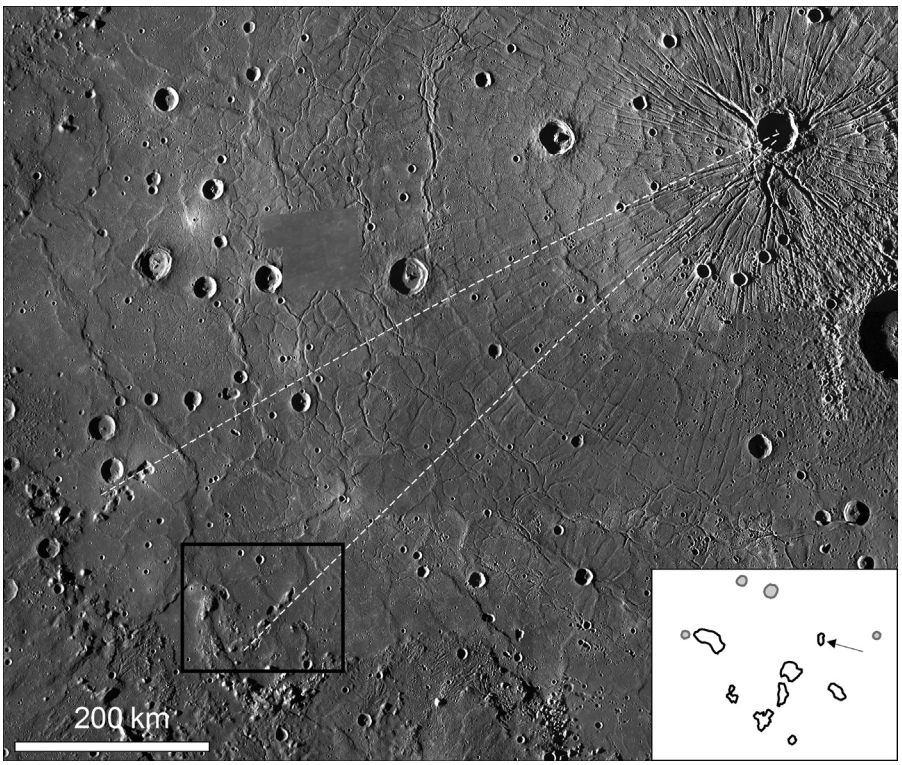


Fig. 8. Sinusoidal projection of part of the MDIS9 mosaic. The two dashed lines are geodesic lines (curved on this map projection) parallel to the vent alignments and consistent with the distal part of Pantheon Fossae radial graben system. The line trending approximately WSW passes through the long axis of the RS-03 vent and is close to all other vents identified in Fig. 2b. The line trending approximately SW passes along a group of four candidate vents within the boxed area. Inset: sketch map of the boxed area. Candidate vents have black outlines, impact craters are shown with a grey fill, as in Fig. 2b. The northeasternmost of the candidate vents in the inset (arrowed) is centred within candidate pyroclastic deposit RS-03 SE of Kerber et al. (2011).

be confused with 'composite volcano' (or composite cone), which denotes construction by alternating lava and pyroclastic materials that may be erupted from a single vent. Fig. 9 shows compound volcanoes on Earth with a similar vent-migration history to RS-03, although there are differences in the mode of caldera/crater formation.

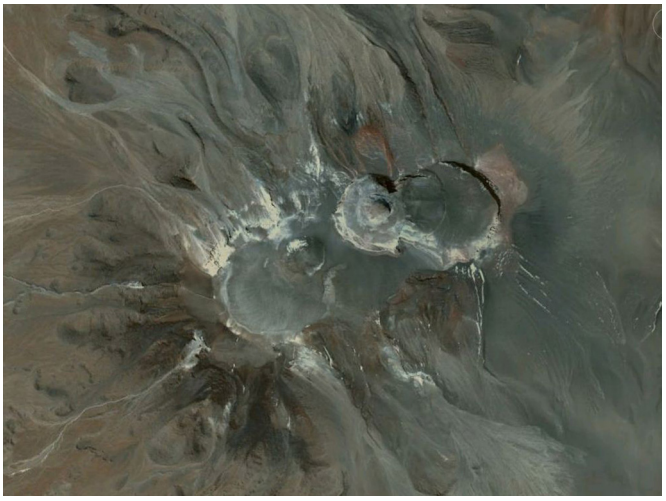
Given that the vents within the RS-03 complex are not flat-floored, but have bowl-shaped or V-shaped profiles, this is a significant contrast with the nested and overlapping calderas on Mars. Those have flat floors and steep, sometimes terraced, walls. Their depressed floors are widely held to result from piston-like subsidence along ring-faults above shallow, deflated magma chambers (e.g., Wilson et al., 2001; Crumpler et al., 1996). In contrast, we suggest that each vent in the RS-03 complex, or at least the younger ones whose forms are essentially unmodified, owes its shape to a combination of explosive excavation of the crater and collapse of the walls of an evacuated conduit, which would at first deepen the main crater floor. Terrestrial examples include the active crater on Telica volcano, Nicaragua (Fig. 10).

We deduce a sequence of vent activity at RS-03 on the grounds of cross-cutting relationships, sharpness versus blurredness of internal texture, and consistent relative densities of impact craters, as follows (using the vent-identification letters in Fig. 2b). Note that this is the sequence of the *most recent* activity at each vent, and does not necessarily reflect the order in which each vent first became active. There may also have been older vents within the perimeter of the complex that have become completely obscured by younger vents. The oldest is A, followed by B then C. D and E are of similar age to each other, and we can find no evidence to decide on the C, D, E sequence. Texture and cross-cutting relationships show that F, G, H and I are the youngest, with their likeliest sequence following the order of lettering.

There is no morphological evidence of lava flows sourced from the vent complex, and shading on the low-Sun WAC image (Fig. 3d) largely disproves the contention of Head et al. (2008) that the eastern rim of the nearby 25 km impact crater has been 'heavily embayed' by eruption products from the RS-03 vent complex. The eastern and northeastern portions of this impact crater rim are shaded/shadowed as would normally be expected, and the rim of this crater appears to be higher than the brink of the RS-03 vent complex. The east to south portion of the impact crater rim has a less clear topographic signature. This could be due to a combination of the influence of Wrinkle Ridge 2 (Fig. 4), which curves towards it, and products erupted from rimless depressions 1 and 4 (Fig. 2b).

The very gentle flank slopes of the RS-03 vent complex are consistent with low-viscosity lavas of the kinds proposed for Mercury on photogeological (Byrne et al., 2013a) and X-ray spectroscopic (Weider et al., 2012) grounds. However, they could also be due largely or even entirely to pyroclastic deposits erupted from each vent. There is actually no evidence that juvenile material played a significant role in the vent-forming pyroclastic events, which could have been essentially vulcanian, driven by volatile escape from subsurface magma but in which the solid eruption products were largely or solely fragments of pre-existing rock. In such a situation the characteristic colour of the candidate pyroclastic products could reflect pre-eruptive subsurface alteration of wall-rock in the presence of hot volatiles rather than the properties of shards of juvenile magma or volcanic glass.

RS-03 cuts across and so post-dates the wrinkle ridge that intersects it. Given the altimetric evidence that wrinkle ridges are topographically more prominent than the very low shield hosting the vent, we would not expect them to be significantly buried by eruption products.



(a)



(b)

Fig. 9. Compound volcanoes on Earth. (a) Volcan Lascar, Chile. Overlapping volcanic craters top an andesitic composite cone volcano that rises more than 2 km above its base. The currently active vent, a site of repeated lava dome growth and collapse, punctuated by explosive eruptions (Gardeweg et al., 1998) is near the centre of the complex. Image is 7 km wide. (b) Volcan Masaya, Nicaragua. Overlapping and nested volcanic craters on a basaltic shield near the centre of a much larger caldera. Present-day activity is gas emission and occasional strombolian explosions at the deep vent on the floor of the crater in the centre left (Rymer et al., 1998). Image is 3 km across.
Source: Google Earth.

We suggest therefore that vent complex RS-03 has a dominantly pyroclastic, explosive, eruptive history, and that it is a structure superimposed on, and therefore post-dating, the Caloris interior plains lavas and their wrinkle ridges. Crater statistics show that Caloris interior plains either post-date the late heavy bombardment (Fassett et al., 2009) or occurred mainly towards the end then possibly continued for 'an undetermined interval' (Strom et al., 2011). The youngest plains surfaces are nevertheless ancient, probably in the region of 3 billion years old. The similarity in sub-1 km size impact crater density on the floor of vent A and on nearby plains is not reliable evidence of similar age because many craters in this small size range are likely to be secondaries (Strom et al., 2011). The smooth and crater-free floors of vents D and E (D has one crater, and E has none) are consistent with these being considerably, conceivably billions of years, younger than the floor of vent A, but do not prove this contention. As an alternative to significant age differences, impact craters on the floors of D and E could have become buried by pyroclastic deposits erupted from vents F–I, but the radial decrease in deposit thickness would need to be surprisingly great for the floors of vents A and B to have escaped a similar fate.



Fig. 10. Volcan Telica, Nicaragua. When photographed in 2000 it was an open-vent degassing volcano, but formerly a site of explosive and effusive eruption of basaltic andesite. The crater lacks a flat floor, and has steep interior slopes leading down to an open vent. Cessation of eruptive activity and further collapse could result in a vent profile similar to that seen in the youngest SW Caloris vents. Internal and external slopes here are steeper than on Mercury. The crater measures approximately 560 m rim to rim at right-angles to the line of sight.

The younger vents, F–I, are smaller than A–E, perhaps reflecting waning eruptive power over time. Their interiors preserve fine-scale texture that has been lost in the older vents, where it could have been mantled by pyroclastic deposits erupted from the younger vents, or become degraded and mantled by regolith-forming processes. Langevin (1997) estimates that on Mercury 5–10 m of regolith should form over 3–4 billion years. The preserved internal morphology of vents F–I does not necessarily represent their state as it was after their last eruption; it could equally likely be a result of the crumbling of conduit walls following magma withdrawal and the collapse of associated caverns. As remarked above, there are no signs of piston-like subsidence along caldera ring-faults.

There are many uncertainties in both absolute age and relative ages. An eruptive lifetime in excess of a billion years at RS-03 is possible, but is poorly constrained. We do not address here the issue of how episodic magmagenesis could have been sustained for such a long period. However, we note that if RS-03 was fed from below from a fixed source, the 25 km spread of the vents suggests that a source depth in excess of 50 km given near-vertical magma or gas ascent.

4.2. The associated vents

Features 4 and 5 (Fig. 2b) are perhaps more similar to the RS-03 vent complex than features 1–3. Feature 4 is the centre of a candidate pyroclastic deposit, and so is very likely to be a site of explosive eruptions like RS-03, whereas 1–3 could be essentially collapse features lacking any erupted products (Gillis-Davis et al., 2009). There are insufficient grounds to regard any of them as 'parasitic' or 'subsidiary' vents (fed by inclined conduits branching off a vertical conduit to a main vent) as opposed to others being 'central' volcanoes. The alignment of the whole suite suggests that it overlies a fracture that is radial to the Caloris basin. There is no definitive evidence of the relative ages, but the internal smoothness of 'feature 5' suggests that it is older than 'feature 4', and this is consistent with the spectral signature of any pyroclastic deposit that once surrounded 'feature 5' having been lost.

5. Conclusions

We interpret the rimless depression centred within the candidate pyroclastic deposit RS-03 as the overlapping vents of a compound volcano, from which eruptions have been dominantly, perhaps exclusively, explosive. The vent complex is at the summit of a subtle edifice whose flanks slope at less than a quarter of a degree. Rimless depressions 40 km to the southwest and 120 km to the northeast (4 and 5 on Fig. 2) may be similar in origin to the RS-03 vent complex. The long axis of the RS-03 vent complex is aligned radially to the Caloris basin, and there is a similar radial alignment within a group of candidate vents to the southeast. Both examples may lie above buried radial fractures that extend much further from the basin centre than the radial fractures that are visible at the surface.

Acknowledgements

We thank Sean Solomon and the MESSENGER Team for their efforts to make newly acquired images publicly available on the MESSENGER website on a regular basis. We are grateful to Carolyn Ernst and an anonymous reviewer for their insightful comments, which helped us to clarify our arguments. D.A.R. acknowledges support from the UK Space Agency in his BepiColombo role.

Appendix A. Supplementary material

Supplementary material related to this article can be found online at http://dx.doi.org/10.1016/j.epsl.2013.10.023.

References

Basilevsky, A.T., Head, J.W., Fasett, C.I., Michael, G., 2011. History of tectonic deformation in the interior plains of the Caloris basin, Mercury. Sol. Syst. Res. 45, 471–497.

Blewett, D.T., Robinson, M.S., Denevi, B.W., Gillis-Davis, J.J., Head, J.W., Solomon, S.C., Holsclaw, G.M., McClintock, W.E., 2009. Multispectral images of Mercury from the first MESSENGER flyby: analysis of global and regional colour trends. Earth Planet. Sci. Lett. 285, 272–282.

Blewett, D.T., Chabot, N.L., Denevi, B.W., Ernst, C.M., Head, J.W., Izenberg, N.R., Murchie, S.L., Solomon, S.C., Nittler, L.R., McCoy, T.J., Xiao, Z., Baker, D.M.H., Fassett, C.I., Braden, S.E., Oberst, J., Scholten, F., Preusker, F., Hurwitz, D., 2011. Hollows on Mercury: MESSENGER evidence for geologically recent volatile-related activity. Science 333, 1856–1859.

Blewett, D.T., Vaughan, W.M., Xiao, Z., Chabot, N.L., Denevi, B.W., Ernst, C.M., Helbert, J., D'Amore, M.D., Maturilli, A., Head, J.W., Solomon, S.C., 2013. Mercury's hollows: Constraints on formation and composition from analysis of geological setting and spectral reflectance. J. Geophys. Res. 118, 1013–1032.

Byrne, P., Klimczak, C., Blair, D., Ferrari, S., Solomon, S., Freed, A., Watters, T., Murchie, S., 2013a. Tectonic complexity within volcanically infilled impact features and basins on Mercury. Lunar Planet. Sci. Conf. 44, 1261.

Byrne, P., Klimczak, C., Blair, D., Ferrari, S., Solomon, S., Freed, A., Watters, T., Murchie, S., 2013b. Tectonic complexity within volcanically infilled impact features on Mercury. Geophys. Res. Abstr. 15, 2173.

Crumpler, L.S., Head, J.W., Aubele, J.C., 1996. Calderas on Mars: characteristics, structure, and associated flank deformation. In: McGuire, W.J., Jones, A.P., Neuberg, J. (Eds.), Volcano Instability on the Earth and Other Planets. In: Spec. Publ., vol. 110. Geol. Soc. London, pp. 307–348.

Davidson, J., de Silva, S., 2000. Composite volcanoes. In: Sigurdssonm, H., Houghton, B., McNutt, S.R., Rymer, H., Stix, J. (Eds.), Encyclopedia of Volcanoes. Academic Press, San Diego, pp. 663–681.

Fassett, C.I., Head, J.W., Blewett, D.T., Chapman, C.R., Dickson, J.L., Murchie, S.L., Solomon, S.C., Watters, T.R., 2009. Caloris impact basin: Exterior geomorphology, stratigraphy, morphometry, radial sculpture and smooth plains deposits. Earth Planet. Sci. Lett. 285, 297–308.

Freed, A.M., Solomon, S.C., Watters, T.R., Phillips, R.J., Zuber, M.T., 2009. Could Pantheon Fossae be the result of the Apollodorus crater-forming impact within the Caloris basin, Mercury? Earth Planet. Sci. Lett. 285, 320–327.

Gardeweg, M.C., Sparks, R.S.J., Matthews, S.S., 1998. Evolution of Lascar Volcano, Northern Chile. J. Geol. Soc. 155, 89–104.

Gillis-Davis, J.J., Blewett, D.T., Gaskell, R.W., Denevi, B.W., Robinson, M.S., Strom, R.G., Solomon, S.C., Sprague, A.L., 2009. Pit-floor craters on Mercury: Evidence of near-surface igneous activity. Earth Planet. Sci. Lett. 285, 243–250.

Hauber, E., Jacob Bleacher, J., Gwinner, K., Williams, D., Greeley, R., 2009. The topography and morphology of low shields and associated landforms of plains volcanism in the Tharsis region of Mars. J. Volcanol. Geotherm. Res. 185, 69–95.

Hawkins, S.E., Boldt, J.D., Darlington, E.H., Espiritu, R., Gold, R.E., Gotwols, B., Grey, M.P., Hash, C.H., Hayes, J.R., Jaskulek, S.E., Kardman, C.J., Keller, M.R., Malaret, E.R., Murchie, S.R., Murphy, P.K., Peacock, K., Prockter, L.M., Reiter, R.A., Robinson, M., Schaefer, E.D., Shelton, R.G., Sterner, R.E., Tayloer, E.D., Watters, T.R., Williams, B.D., 2007. The Mercury Dual Imaging System on the MESSENGER spacecraft. Space Sci. Rev. 131, 247–338.

Head, J.W., Murchie, S.L., Prockter, L.M., Robinson, M.S., Solomon, S.C., Strom, R.S., Chapman, C.R., Watters, T.R., McClintock, W.E., Blewett, D.T., Gillis-Davis, J.J., 2008. Volcanism on Mercury: Evidence from the first MESSENGER flyby. Science 321, 69–72.

Head, J.W., Murchie, S.L., Prockter, L.M., Solomon, S.C., Chapman, C.R., Strom, R.G., Watters, T.R., Blewett, D.T., Gillis-Davis, J.J., Fassett, C.I., Dickson, J.L., Morgan, G.A., Kerber, L., 2009. Volcanism on Mercury: Evidence from the first MESSENGER flyby for extrusive and explosive activity and the volcanic origin of plains. Earth Planet. Sci. Lett. 285, 227–242.

Kerber, L., Head, J.W., Solomon, S.C., Murchie, S.L., Blewett, D.T., Wilson, L., 2009. Explosive volcanic eruptions on Mercury: Eruption conditions, magma volatile content, and implications for interior volatile abundances. Earth Planet. Sci. Lett. 285, 263–271.

Kerber, L., Head, J.W., Blewett, D.T., Solomon, S.C., Wilson, L., Murchie, S.L., Robinson, M.S., Denevi, B.W., Domingue, D.L., 2011. The global distribution of pyroclastic deposits on Mercury: The view from MESSENGER flybys 1–3. Planet. Space Sci. 59, 1895–1909.

Langevin, Y., 1997. The regolith of Mercury present knowledge and implications for the Mercury Orbiter mission. Planet. Space Sci. 45, 31–37.

McEwen, A.S., Bierhaus, E.B., 2006. The importance of secondary cratering to age constraints on planetary surfaces. Annu. Rev. Earth Planet. Sci. 34, 535–567.

Murchie, S.L., Watters, T.R., Robinson, M.S., Head, J.W., Strom, R.S., Chapman, C.R., Solomon, S.C., McClintock, W.E., Prockter, L.M., Domingue, D.L., Blewett, D.T., 2008. Geology of Caloris basin, Mercury: A view from MESSENGER. Science 321, 73–76.

Oberst, J., Preusker, F., Phillips, R.J., Watters, T.R., Head, J.W., Zuber, M.T., Solomon, S.C., 2010. The morphology of Mercury's Caloris basin as seen in MESSENGER stereo topographic models. Icarus 209, 230–238.

Rymer, H., van Wyk de Vries, B., Stix, J., Williams-Jones, G., 1998. Pit crater structure and processes governing persistent activity at Masaya Volcano, Nicaragua. Bull. Volcanol. 59, 345–355.

Spudis, P.D., McGovern, P.J., Kiefer, W.S., 2013. Large shield volcanoes on the Moon. J. Geophys. Res. 118, 1063–1081.

Strom, R.G., Banks, M.E., Chapman, C.R., Fassett, C.I., Forde, J.A., Head, J.W., Merline, W.J.H., Prockter, L.M., Solomon, S.C., 2011. Mercury crater statistics from MESSENGER flybys: Implications for stratigraphy and resurfacing history. Planet. Space Sci. 59, 1960–1967.

Thomas, R.J., Rothery, D.A., Conway, S.J., Anand, M., 2013. Mechanisms and sources involved in the formation of hollows on the surface of Mercury. Lunar Planet. Sci. Conf. 44 (abstract 1182).

Watters, T.R., Murchie, S.L., Robinson, M.S., Solomon, S.C., Denevi, B.W., André, S.L., Head, J.W., 2009. Emplacement and tectonic deformation of smooth plains in the Caloris basin, Mercury. Earth Planet. Sci. Lett. 285, 309–319.

Weider, S.Z., Nittler, L.R., Starr, R.D., McCoy, T.J., Stockshill-Cahill, K.R., Byrne, P.K., Denevi, B.W., Head, J.W., Solomon, S.C., 2012. Chemical heterogeneity on Mercury's surface revealed by the MESSENGER X-ray spectrometer. J. Geophys. Res. 117, E00L05, http://dx.doi.org/10.1029/2012JE004153.

Wilson, L., Scott, E.D., Head, J.W., 2001. Evidence for episodicity in the magma supply to the large Tharsis volcanoes. J. Geophys. Res. 106, 1423–1433.

Zuber, M.T., Smith, D.E., Phillips, R.J., Solomon, S.C., Neumann, G.A., Hauck, S.A., Peale, S.J., Barnouin, O.S., Head, J.W., Johnson, C.L., Lemonine, F.G., Mazarico, E., Sun, X., Torrence, M.H., Freed, A.M., Klimczak, C., Margot, J.-L., Obserst, J., Perry, M.E., McNutt, R.L., Balcerski, J.A., Michel, N., Talpe, M.J., Yang, D., 2012. Topography of the northern hemisphere of Mercury from MESSENGER laser altimetry. Science 326, 217–220.